

Space charge effects in field emission: One dimensional theory

A. Rokhlenko,¹ K. L. Jensen,^{2,a)} and J. L. Lebowitz^{1,3}

¹*Department of Mathematics, Rutgers University, Piscataway, New Jersey 08854-8019, USA*

²*Code 6843, ESTD, Naval Research Laboratory, Washington, DC 20375-5347, USA*

³*Department of Physics, Rutgers University, Piscataway, New Jersey 08854-8019, USA*

(Received 15 June 2009; accepted 10 November 2009; published online 5 January 2010)

The current associated with field emission is greatly dependent on the electric field at the emitting electrode. This field is a combination of the electric field in vacuum and the space charge created by the current. The latter becomes more important as the current density increases. Here, a study is performed using a modified classical one dimensional (1D) Child–Langmuir description that allows for exact solutions in order to characterize the contributions due to space charge. Methods to connect the 1D approach to an array of periodic three dimensional structures are considered.

© 2010 American Institute of Physics. [doi:10.1063/1.3272690]

INTRODUCTION

Space charge, or the effects of Coulomb interactions between emitted electrons, and its impact on the generation and transport of electron beams are important in many practical applications, particularly when beam brightness and modulation characteristics are critical to the operation of the device. Consequently, both space charge and emittance dominated beams have received intense study, particularly as they relate to thermal and photoemission sources for amplifiers and particle accelerators.^{1–6} In contrast, field emission relies on quantum mechanical tunneling through barriers thinned through the application of fields on the order of 10 GV/m at the emission site. As the highest macroscopic fields that can be generated are smaller (100 MV/m for rf photoinjectors, 1–50 MV/m for vacuum electronic devices, etc.) field enhancement must be utilized by making the emission sites have sharp features.^{7,8} While field emitters that resemble pyramids, ellipsoids, or whiskers⁹ in microfabricated arrays¹⁰ boast current densities at the emission sites many orders of magnitude larger than for thermal and photoemission sources, the emission area is generally on the order of 100 nm² per site. The high curvature of the site geometry makes modeling of field emitters in modern particle-in-cell (PIC) codes an issue: simple models of space charge or emittance from these sources are unable to fully exploit the one dimensional (1D) techniques often used in the analysis of other electron sources or treat many separate emitters acting in concert. Nevertheless, there have been several theoretical efforts:^{11–16} in particular, the treatment of the 1D field emission/space charge problem (Ref. 17 and references therein), the usage of PIC codes to treat field emission (Ref. 18 and references therein) and the discussion of numerical issues involved in modeling space-charge-limited flow (even in the 1D case using PIC codes can lead to unusual behavior as a consequence of cell-size related problems),¹⁹ that are pertinent.

The present study is the first of a two part effort to describe the coupling of 1D and three dimensional (3D) ap-

proaches to field emission in a manner that allows for the effects of space charge on the operation of microfabricated structures to be addressed. Here, a methodology for the analysis of space charge forces on the emission process is described, and a manner in which 1D methods may be brought to bear on arrays of emitters operating together is presented (the second, and separate, study concerns the impact of space charge on individual 3D structures and builds on methods introduced in the analysis of dark current²⁰ and emittance.²¹ The objective is to provide a framework to investigate field emitters without intensive numerical efforts in a manner amenable to PIC codes for when space charge is an issue and the cathode area is but a small region of the simulation. Applications that rely on field emission will benefit, and such applications include (but are not limited to) electron beam lithography^{22,23} and transmission electron microscopes,²⁴ spacecraft propulsion,^{25,26} millimeter-wave vacuum electronic amplifiers and terahertz devices,^{27,28} and particle accelerators and free electron lasers (FELs).^{29–31}

THE 1D MODEL

Poisson's equation in one dimension can be written

$$\frac{d^2}{dx^2}V(x) = \frac{q^2}{\epsilon_0}\rho, \quad (1)$$

where q is the elementary charge, ρ is a number density, and $V(x)$ is potential energy. The current density J is given by

$$J = qv\rho = q\rho\left(\frac{2V}{m}\right)^{1/2}, \quad (2)$$

where (as in Table I) v is the electron velocity and m is the electron mass. The second equality comes from the assumption that the velocity is zero at the cathode where $V=0$. Introduce the dimensionless quantities φ , y , and j such that

$$V = \varphi V_0,$$

$$J = jJ_0,$$

^{a)}Electronic mail: kevin.jensen@nrl.

TABLE I. Symbols and parameters.

Symbol	Definition	Value	Unit
Fundamental constants and parameters			
m	Electron mass	510 999	eV/c ²
c	Speed of light	299.792	nm/fs
\hbar	Planck's constant	0.658 212	eV fs
q	Unit charge	1	q
R_∞	Rydberg constant	13.605 7	eV
α_{fs}	Fine structure constant	1/137.036	...
a_o	Bohr radius $\hbar/\alpha_{fs}mc$	0.052 917 7	nm
ϵ_0	Permittivity of free space	$5.526\ 35 \times 10^{-2}$	$q^2/\text{eV nm}$
Q	$\alpha_{fs}\hbar c/4$	0.359 991	eV nm
F	Field at cathode	...	eV/nm
V	Potential	...	eV
Copperlike parameters			
μ	Chemical potential	7	eV
k_F	$(2m\mu)^{1/2}/\hbar$	13.554 6	1/nm
v_F	Fermi velocity	1.569 19	nm/fs
Φ	Work function	4.5	eV
FN field emission parameters			
B	J_{FN} parameter, Eq. (20)	65.207 3	eV/nm
κ	J_{FN} parameter, Eq. (20)	0.772 808	...
$v(y)$	Elliptical integral function	$1-y^2[1-\frac{1}{3}\ln(y)]$...
$t(y)$	Elliptical integral function	$\approx t(y_o)=1.061$...
y_o	$e^{-1/2}$	0.606 531	...

$$x = yL, \quad (3)$$

where V_o is the anode potential, J_o is a characteristic current, and L is the distance between the anode and the cathode surface. Equation (1) becomes (compare to the treatments of Refs. 32 and 33)

$$\frac{d^2}{dy^2}\varphi(y) = \frac{j}{\sqrt{\varphi}}, \quad (4)$$

where J_o is defined by

$$J_o \equiv \frac{9}{4}J_{CL}(V_o, L) = \sqrt{\frac{2}{m}} \left(\frac{\epsilon_o V_o^{3/2}}{qL^2} \right) \quad (5)$$

and J_{CL} is the familiar Child–Langmuir (CL) maximum current that can be drawn across an anode-cathode gap with no initial velocity of the electrons and zero field at the cathode.³ Solving Eq. (4) with appropriate boundary conditions is straightforward and has been done in the literature (see Ref. 17 and references therein), but the solution is synopsised in the present notation with an eye to eliminate problems with the appearance of nonphysical results. Representing the product of charge q and field at the cathode by $F=fV_o/L$, where f is dimensionless, solutions to Eq. (4) are then given by

$$\frac{d\varphi}{dy} = (4j\sqrt{\varphi} + f^2)^{1/2}. \quad (6)$$

A second integration yields [compare Eq. (3) of Ref. 11]

$$(4j\sqrt{\varphi} + f^2)^{1/2}(2j\sqrt{\varphi} - f^2) + f^3 = 6j^2y. \quad (7)$$

Invoking the boundary conditions that at $y=1$, $\varphi=1$, then gives

$$(4j + f^2)^{1/2}(2j - f^2) + f^3 = 6j^2. \quad (8)$$

Equation (8) is an exact equation for the 1D diode and does not have unphysical solutions: manipulations with it should be done with care in order not to introduce them. Equation (8) can be written as

$$j = \frac{1}{9}[2 + (2 - 3f)\sqrt{1 + 3f}], \quad (9)$$

which provides a universal relation between the current and the field at the cathode independent of the relation between the field at the cathode and the emitted current (see also Ref. 17). It encapsulates the two most familiar limits: in the limit that the current vanishes, then $f=1$, or the field at the cathode $F=V_o/L$; conversely, if $f=0$, then $j=4/9$ (the CL current density). Observe that the field f at the cathode cannot exceed 1 (its vacuum value) when space charge is absent and there is no screening.

We shall consider particular solutions depending on the behavior of $j(f)$, namely, a linear and quadratic dependence, which can be handled analytically, and a Fowler–Nordheim (FN) linear field model.³⁴ Using the image charge, or Schottky barrier lowering, factor³⁵ is reserved for the 3D case and shall be considered separately.³⁶ Before considering these cases, we note that Eq. (8) can be manipulated and re-expressed in a convenient form without square roots as

$$3f^2(1 - f) - j(4 - 9j) = 0, \quad (10)$$

which bears a relationship to Eq. (13) of Forbes¹⁷ [note, however, that Eq. (10) allows unphysical solutions as the second root of the resulting quadratic equation, e.g., $f=1$ and $j=4/9$, satisfies Eq. (10) but is not a solution of Eq. (8)].

Linear current-field relationship

For $j=af$, that is, the current is linear in the cathode surface field, then according to Eq. (10) the field satisfies

$$0 = 3f^2(1 - f) - af(4 - 9af). \quad (11)$$

The physically relevant solution is given by

$$f = \frac{1}{2} \left\{ 1 + 3a^2 + (1 - 3a)\sqrt{1 + \frac{2}{3}a + a^2} \right\}, \quad (12)$$

which yields $f=1$ when $a=0$ (and thus $j=0$). The case $a=1/3$ corresponds to $f=2/3$ and $j=2/9$ (half of the space charge limit). The behavior of Eq. (12) is shown in Fig. 1 in a form that shows the asymptotic convergence of f to the CL limit: the y -axis is the ratio of $j=af$ with the space charge limit $j_{CL}=4/9$. The increasing influence of space charge can be seen in the small a limit, whereas the approach to space charge limited current can be seen in the large a limit: these limits are

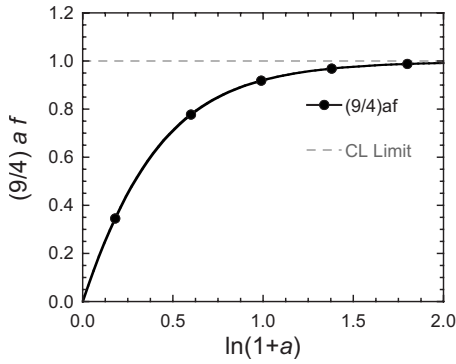


FIG. 1. Behavior of f as given by Eq. (12) for the linear current-field relationship (the gray dashed line represents the CL limit).

$$j(a \ll 1) \approx \frac{a}{1 + \frac{4}{3}a + \frac{5}{9}a^2},$$

$$j(a \gg 1) \approx \frac{4}{9 + \frac{4}{a^2}}. \tag{13}$$

The expansions are reasonably good: at $a=1$ Eq. (13) suggests that $j \approx 0.346$ and 0.333 for the small and large expansions, respectively, as compared to the exact value $j=0.367$,

Quadratic current field

When $j=af^2$, then Eq. (10) becomes

$$0 = f^2[3(1 - f) - a(4 - 9af^2)]. \tag{14}$$

The physical solution of Eq. (14) is

$$f = \frac{1}{6a^2}[1 - (1 - 2a)\sqrt{4a + 1}]. \tag{15}$$

The behavior of the current $j=af^2$ found from Eq. (15) is shown in Fig. 2 in a form that exhibits its asymptotic convergence to the CL limit as done in the linear case. As before, the influence of space charge in the small and large a limits are

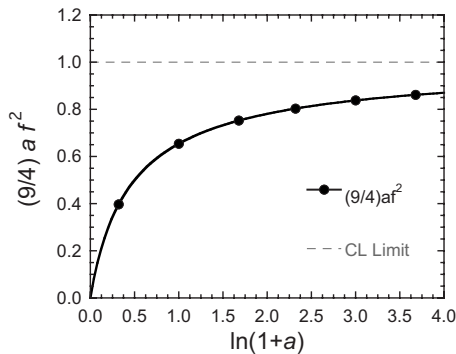


FIG. 2. Behavior of f as given in Eq. (15) for the quadratic current-field relationship (the gray dashed line represents the CL limit).

$$j(a \ll 1) \approx \frac{a}{1 + \frac{8}{3}a - \frac{2}{3}a^2},$$

$$j(a \gg 1) \approx \frac{4}{9 + \frac{4}{a}}. \tag{16}$$

where Eq. (16) suggests that at $a=1$, $j \approx 0.333$, and 0.254 for the small and large expansions, respectively, as compared to the exact value $j=0.291$. Also, observe that f is approximately unity for small values of a : specifically, to leading order in a , then $f(a \ll 1) = 1 - (4a/3)$ for both the linear and quadratic cases.

The question of what values of the parameters determine when the current becomes space charge dominated is very important in practice. For the 1D geometry and the simple emission models considered, the answers appear in Figs. 1 and 2: the current is half of the CL limit (i.e., $j=2/9$) when $a=1/3$ and $1/2$ for the linear and quadratic dependences, respectively. These quantities can be easily related to physical units by using Eq. (3).

FN current-field relation

For the triangular barrier, the FN current-density versus field relationship $J_{FN}(F)$ [i.e., Eq. (8) of Ref. 35] can be expressed as

$$j = \frac{J_{FN}(F)}{J_o} \equiv af^2 \exp\left(-\frac{b}{f}\right), \tag{17}$$

where

$$a = \frac{1}{\pi(\mu + \Phi)} \sqrt{\frac{\mu R_z V_o}{\Phi}},$$

$$b = \frac{4}{3} \left(\frac{L}{a_o}\right) \left(\frac{\Phi}{V_o}\right) \sqrt{\frac{\Phi}{R_z}}, \tag{18}$$

and terms are as defined in Table I. The work function Φ is, in the absence of the image charge, equivalent to the height of the triangular barrier above the Fermi energy μ for a metal. The form of Eq. (18) makes the dimensionless nature of a and b transparent. Their dependence on the anode potential V_o may give pause, but recall that the current density depends on the field strength at the cathode (i.e., f) rather than the anode potential, and that j is scaled by the CL result. Equation (8) can be written as

$$(4j + f^2)^{1/2} = \frac{6j^2 - f^3}{2j - f^2}. \tag{19}$$

The denominator vanishes for $j=f^2/2$. For the left hand side is finite, the numerator must vanish, or $f^3=(3/2)f^4$. Thus, the degenerate root in the FN case is given by $f=2/3$ and $j=2/9$ (half of the CL limit). In mksa units, this will occur when

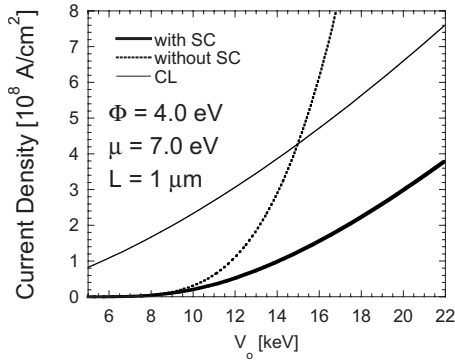


FIG. 3. Onset of space charge effects for a high (4.0 eV) work function for the 1D field emission current density assuming a 1 μm anode to cathode separation, metal-like parameters, and a triangular barrier [no Schottky barrier lowering—Eq. (17)]. The dashed line represents the FN equation with $F=V_0/L$; the solid thick line therefore corresponds to $F=fV_0/L$ and therefore includes the effects of space charge.

$$V_{\text{trans}} = \frac{2\Phi \left(\frac{L}{a_0}\right) \sqrt{\frac{\Phi}{R_\infty}}}{\ln \left[\frac{2}{\pi(\mu + \Phi)} \sqrt{\frac{\mu R_\infty V_{\text{trans}}}{\Phi}} \right]}, \quad (20)$$

which can be solved iteratively. For example, for $L=1 \mu\text{m}$, $\mu=7 \text{ eV}$, and $\Phi=4 \text{ eV}$, then V_{trans} converges to 21.953 keV after eight iterations for a starting guess of 10 keV. V_{trans} therefore serves as a transition point between when one branch of the numerical solution of $j_{\text{FN}}(f)$ is taken ($V < V_{\text{trans}}$) versus the other ($V > V_{\text{trans}}$): this affects, for example, the maximum and minimum V considered in a bisection method to find the current density, as in the first branch V_{trans} is the larger value, whereas in the second branch, it is the smaller. For an L of 1 μm the impact of space charge on the current density versus anode potential is shown in Fig. 3 for metal-like parameters. Field emission results are more conventionally shown on a FN plot of $1/V$ versus $\ln[J_{\text{FN}}(V)/V^2]$, and so the data of Fig. 3 are recast in that form in Fig. 4 with V in keV and J in A/cm^2 . The impact of lowering the work function to 2.0 and 0.5 eV is shown in Figs. 5 and 6, respectively. The departure from linearity on such plots indicates the impact of space charge forces.

Current regimes: Limiting cases

Small current

Small values of a in the linear, quadratic, and more general cases such as FN correspond to small j , and therefore,

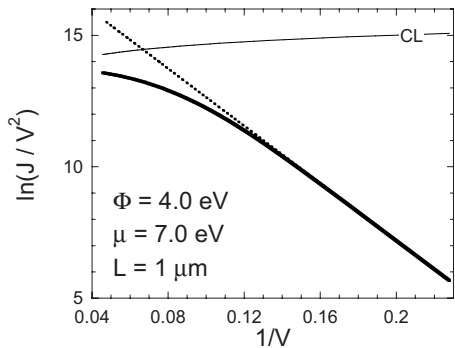


FIG. 4. Same as Fig. 3, but for the data represented on a traditional FN plot.

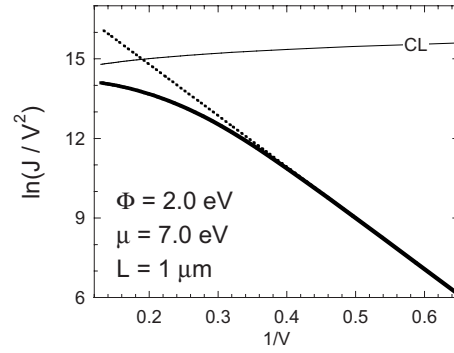


FIG. 5. Same as Fig. 4, but for a middle (2.0 eV) work function. The thin line labeled “CL” is the Child-Langmuir limit [see Eq. (5)].

Eqs. (13) and (16) for j for more general relations can be obtained from an expansion of Eq. (9) for small $(1-f)$: to second order

$$j(f \approx 1) \approx \frac{3}{4}(1-f) - \frac{15}{64}(1-f)^2. \quad (21)$$

In conjunction with a Taylor expansion of $j(f)$ for f near unity given by

$$j(f) = j(1) - (1-f)j'(1), \quad (22)$$

where prime indicates derivative with respect to argument, then to leading order,

$$j(f) \approx \frac{j(1)}{1 + \frac{4}{3}j'(1)} \equiv \frac{j(1)}{1 + \epsilon}, \quad (23)$$

which is equivalent (to order a) to Eqs. (13) and (16) with regards to the denominator. For the FN $j(f)$ then Eqs. (17) and (23) imply

$$\epsilon_{\text{FN}} \approx \frac{8}{3}ae^{-b} \quad (24)$$

and arises from increasing space charge when the cathode efficiency (larger a and smaller b) is larger.

The correction factor ϵ_{FN} that arises from space charge is not difficult to examine experimentally because strong field emission is not required. Importantly, if the anode potential V_0 and the anode-cathode separation L are changed such that their ratio $F=V_0/L$ remains constant, then by virtue of the definition of ϵ_{FN} and j , it is seen

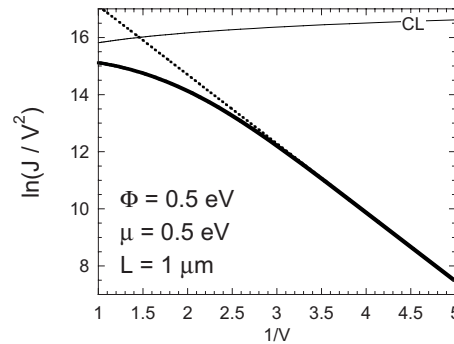


FIG. 6. Same as Fig. 4, but for a small (0.5 eV) work function and small (0.5 eV) chemical potential.

$$\varepsilon_{\text{FN}} = \frac{1}{3}(b+2) \frac{J_{\text{FN}}(F)}{J_{\text{CL}}\left(V_o, L = \frac{V_o}{F}\right)} \quad (25)$$

and so because $J_{\text{CL}}(V_o, F/V_o)$ scales as $V_o^{-1/2}$, it is seen that ε_{FN} scales as $V_o^{1/2}$.

Large current

When the current density is large and $j(f)$ of a more complex form [e.g., Eq. (17)], then numerical methods are required to solve Eq. (8). However, if emission is so large that f is small, then from Eq. (9) it follows that

$$j = j_o - f^2 \frac{(2 + \sqrt{3f+1})}{(1 + \sqrt{3f+1})^2} \approx j_o - \frac{3}{4}f^2, \quad (26)$$

where [from Eq. (5)] $j_o = 4/9$. That is, when $f > 1/4$, then j is greater than 90% of the CL limit without much regard to the details of the dependence of j on f .

For small f and constant V_o/L , then the variation in j with a for the linear (l), quadratic (q), and FN relationships behave as

$$\begin{aligned} \partial_a j_l &= f, \\ \partial_a j_q &= f^2, \\ \partial_a j_{\text{FN}} &= f^2 e^{-bf}. \end{aligned} \quad (27)$$

We note that for small f there is a decrease in the magnitude of these derivatives which manifests itself in a slower approach to the CL limit (see Figs. 1 and 2).

Comparison to PIC simulations

PIC codes are widely used methods to analyze the impact of space charge forces on beam transport. Electrons can be launched into the anode-cathode gap region, and their presence introduces fields that impede subsequent emission, especially if the emission is dependent on the field at the cathode surface. Although time dependent phenomena, particularly in the form of oscillations in the current density, are to be expected, such variations damp out and a steady state equilibrium can be approached. PIC simulations addressing field emission have been performed by Feng and Verboncoeur:¹⁸ they examined the approach of field emission to space charge limited flow in a 1D simulation. Here, the findings of Feng and Verboncoeur are compared to predictions based on solutions to Eq. (9).

There are differences between the emission model used by Feng and Verboncoeur and the triangular barrier model of the original FN equation: an image charge corrected form of the FN equation is employed by the PIC simulations in which the barrier is lowered by a Schottky factor by $\Delta\Phi = \sqrt{\alpha_{\text{fs}} \hbar c F}$. Therefore, the height of the barrier above the Fermi level μ is given by

$$\phi = \Phi - \sqrt{\alpha_{\text{fs}} \hbar c F} \equiv (1-y)\Phi \quad (28)$$

which defines the term y . As discussed by Murphy and Good,⁸ the primary impact of the Schottky factor is to alter the a and b factors in Eq. (17) by appending $t(y)^{-2}$ to the

former and $v(y)$ to the latter (and will be treated in greater detail in the second study³⁶): the intention here is to compare the 1D theory of Eq. (10) to the PIC simulations of Feng and Verboncoeur, and so their approximations shall be used temporarily. However, as discussed by Forbes,³⁷ $F_{\text{max}} = \Phi^2 / \alpha_{\text{fs}} \hbar c$ corresponds to that field which lowers the emission barrier to the Fermi level (i.e., $\phi=0$): thus, in the usage of the FN equation with image charge correction, fields larger than F_{max} are disallowed by the approximations from whence the FN equation is derived.³⁸ If the largest field considered is 10 GV/m, then the work function must be larger than 3.8 eV. As a result, only the findings summarized in Fig. 11 of Ref. 18 for which the work function is 4 eV and the anode-cathode separation is 1 μm are considered.

As shown elsewhere,^{39,40} the impact due to changes in a tunneling barrier shape on the exponential term in the FN equation is captured in the factor $v(y)$ (for the image charge potential) or analogs to it. That is, the image charge barrier FN equation can be made to resemble the triangular barrier FN equation if the effective work function Φ_{eff} depends on the field F . From Eq. (18), it is seen that the exponential term of the triangular barrier FN equation scales as $b \propto \Phi^{3/2}$. Equating the exponential arguments of the triangular barrier FN equation with the image charge form, it is seen

$$\Phi_{\text{eff}}^{3/2} = \Phi^{3/2} v \left(\frac{1}{\Phi} \sqrt{\alpha_{\text{fs}} \hbar c F} \right). \quad (29)$$

The coefficient of the exponential terms in both the triangular and image charge FN equations have different dependences on the work function parameter. In keeping with the “effective” work function concept, a factor of C is appended to the triangular FN equation. A naive equivalence between the triangular and effective equations then suggests

$$C \approx \frac{1}{4\Phi l(y)^2} \left(\frac{\Phi_{\text{eff}}}{\mu} \right)^{1/2} (\mu + \Phi_{\text{eff}}), \quad (30)$$

which, for copperlike parameters and fields of 3 GV/m (the image charge barrier more closely resembles a triangular barrier for low field) is $C \approx 0.42$. Because the equivalence is not exact (an effective work function only roughly relates an image charge barrier to a triangular barrier) it can only be concluded that C is on the order of 1/2.

Solutions of Eq. (10) using Eq. (17) for $j(f)$, and Eq. (18) for a and b for which Φ is replaced by Φ_{eff} as per Eq. (29) were calculated. The final j was then scaled by the factor $C=1/2$. Observe that scaling by C does not make the scaled j [the solution of Eq. (9)] the same as the space charge limited FN current found by Feng and Verboncoeur: the scaling is only to show that the 1D triangular barrier FN equation used in Eq. (9) anticipates the image charge FN equation in that their dependence on F is qualitatively comparable. Using the approximation Feng and Verboncoeur use of $v_{\text{FV}}(y) \approx 1-y$ ^{1,69}, the results of the comparison are shown in Fig. 7: the combination of an effective work function and a scaling parameter anticipates the PIC simulations remarkably well, demonstrating that the 1D solution using the triangular barrier FN equation is, in fact, a good predictor (albeit not a replacement) of the behavior to be found using the image

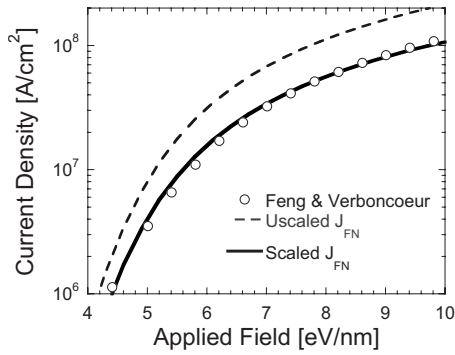


FIG. 7. Comparison of the space charge limited current as a function of applied field (ratio of anode voltage to anode-cathode separation) data of Fig. 11(a) of Ref. 18 (“Feng and Verboncoeur”) to Eq. (10) using the effective work function Φ_{eff} of Eq. (29) without (“unscaled J_{FN}”) and with (“scaled J_{FN}”) $C=1/2$: see discussion following Eq. (30).

charge FN equation in PIC simulations to within a scale factor C for the space charge limited current.

The triangular barrier FN equation was used so that small work function potentials could be considered without running afoul of the Schottky factor lowering the emission barrier to below the Fermi level. Not only for small barriers but also for barriers, in general, the j of Eq. (9) can be suitably modified to accommodate situations where temperature and/or field make the emitted current density complex and possibly temperature dependent (e.g., the general thermal field equation given by Eq. (36) of Ref. 41).

Connection of the 1D model to an array

The 1D model regards emission of uniform sheets of charge from a surface.⁴² Field emission arrays, in contrast, emit from a lattice of emitter sites. As is well known in electrostatics (and explicitly utilized by the point charge model^{20,21}), conducting surfaces can be replaced by equipotential surfaces at the same potential, and the converse holds as well: the equipotential surface signifying “anode” in the point charge model becomes the “cathode” of the 1D region,

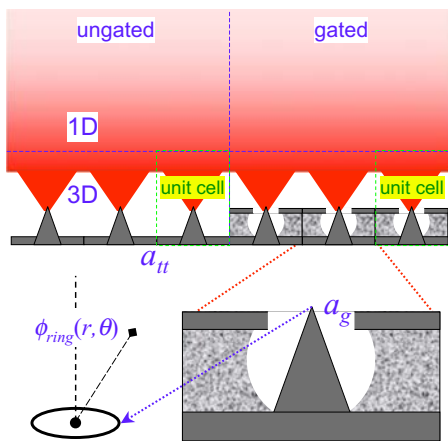


FIG. 8. (Color online) Schematic of an array of emitters in the ungated (left) and gated (right) configurations. The 1D approach applies for large z (top) and the unit cell approach for small z (bottom). An enlargement of the gated emitter is shown on the bottom right, and its Saturn model representation on the bottom left, where the point and ring charges are in the gate plane.

as schematically illustrated in Fig. 8. How far from the plane of charges the anode in the point charge model must be before the discrete nature of the PCM is sufficiently smoothed to approximate the planar cathode in the 1D approach is now investigated.

Consider a sheet of point charges spaced on a square grid for which the tip-to-tip distance is a_{tt} (alternately, the pitch of the array) and the magnitude of each charge is proportional to λ : by superposition, the sheets due to the other λ 's can be considered separately and combined afterward. Express all lengths in units of a_{tt} and to take the cathode surface to be at $z=0$ and the anode to be at $z=N/2$ and far away ($N \gg 1$). For the anode potential to be constant and uniform, image charges of equal and opposite sign to the cathode point charges are placed at $z=N$. The potential everywhere between $0 < z < N/2$ is then given by

$$V(x, y, z) = V_0 + \frac{\lambda}{4\pi\epsilon_0 a_{\text{tt}}} \sum_{j=-\infty}^{\infty} \sum_{k=-\infty}^{\infty} \varphi_{jk}(x, y, z),$$

$$\varphi_{jk}(x, y, z) = \frac{1}{R_c} - \frac{1}{R_a} = \frac{R_a^2 - R_c^2}{R_a R_c (R_a + R_c)} = \frac{N(N-2z)}{R_c R_a (R_c + R_a)},$$

$$R_c = [(j-x)^2 + (k-y)^2 + z^2]^{1/2},$$

$$R_a = [(j-x)^2 + (k-y)^2 + (N-z)^2]^{1/2}, \quad (31)$$

where the ordering of the arguments in φ reflect that the potential satisfies $V(x+n, y+m, z) = V(x, y, z)$ for integers n and m , and therefore x and y may be assumed less than $1/2$. For computational purposes, the last form of $\varphi_{i,j}$ in Eq. (31) is preferred. Likewise, the z component of the field is given by

$$\hat{z} \cdot \mathbf{F}(x, y, z) = \frac{\lambda}{4\pi\epsilon_0 a_{\text{tt}}^2} \sum_{j=-\infty}^{\infty} \sum_{k=-\infty}^{\infty} \varphi'_{jk}(x, y, z),$$

$$\varphi'_{jk}(x, y, z) \equiv \frac{z}{R_c^3} + \frac{N-z}{R_a^3}. \quad (32)$$

The other components are analogous, but the z component is dominant. How large must z be before the point particle nature of the charges is obscured sufficiently to approximate the 1D framework is the question.

Consider a finite circular array of point charges of diameter $2M$ such that Eq. (31) is the $M \rightarrow \infty$ limit. It is expedient to numerically analyze finite M and generalize to the $M \rightarrow \infty$ case. For z sufficiently large that the series can be well approximated by an integral, it follows

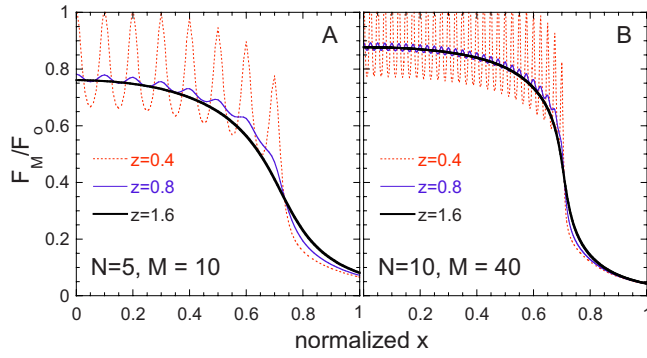


FIG. 9. (Color online) The z component of the gradient of the potential along the diagonal defined by $x=y$ for a circular emitters arranged on a square grid with $(N,M)=(5,10)$ for the left (a), and $(10,40)$ for the right (b) for various values of z (red (dashed)=0.4, blue (thin line)=0.8, black (thick line)=1.6). The length is scaled by half of the diagonal of the total square region (that is, $\sqrt{2M}$). For infinite uniform charged parallel plates, the field between them would be constant (independent of z) and equal to F_o .

$$\hat{z} \cdot \mathbf{F} = \lim_{M \rightarrow \infty} F_M,$$

$$\begin{aligned} \frac{F_M}{F_o} &= \frac{1}{4\pi} \sum_{j=-M}^M \sum_{k=-\sqrt{M^2-j^2}}^{\sqrt{M^2-j^2}} \varphi'_{j,k}(z) \\ &\approx \frac{1}{2} \int_0^M \left\{ \frac{zr}{(r^2+z^2)^{3/2}} + \frac{(N-z)r}{[r^2+(N-z)^2]^{3/2}} \right\} dr \\ &= 1 - \frac{z}{2\sqrt{M^2+z^2}} - \frac{(N-z)}{2\sqrt{M^2+(N-z)^2}}, \end{aligned} \quad (33)$$

where $F_o = \lambda / \epsilon_0 a_{tt}^2$. It is seen that the second two terms in the third line of Eq. (33) are equivalent to

$$\frac{z}{2\sqrt{M^2+z^2}} + \frac{(N-z)}{2\sqrt{M^2+(N-z)^2}} = \frac{1}{2} \int_M^\infty r dr \varphi'_{jk}(z)|_{j^2+k^2=r^2}. \quad (34)$$

For $M \gg N > z$, then to leading order the z component of field is $F = F_o[1 - (N/2M)]$. Clearly, as $M \rightarrow \infty$, F approaches the parallel plate solution F_o . The finite M form of Eq. (32) can be evaluated numerically, and how large z should be can be inferred from when Eq. (33) approaches its $1 - (N/2M)$ limit. Consider the variation in F_M/F_o given by Eq. (33) along the line $x=y$, for which variations are at their maximum, for representative values of (N,M) of $(5,10)$ and $(10,40)$ in Fig. 9. For $z > 1$, the undulations in F_z are largely absent. This can also be seen in the behavior of the potential itself in Fig. 10 for (N,M) values of $(4,8)$ at $z=0.4$ (A) and $z=1.6$ (B): the color scales differ as the potential increases with z , but it is clear that the collection of pointlike potentials for $z < 1$ merges into a more uniform, or sheetlike, behavior for $z > 1$. The small values of N and M are to facilitate visual inspection, but field emitter arrays are characterized by far larger M than considered herein, for which F_z is more nearly constant within the disk defining the active array area. Consequently, z values of order unity are the appropriate locations for which to transition from a unit cell representation (discussed separately³⁶) to the 1D approach, with the anode

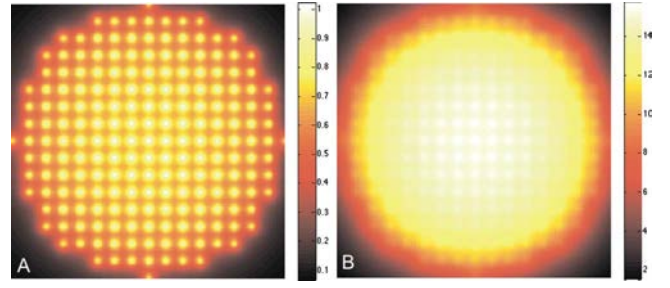


FIG. 10. (Color online) Same as Fig. 9, but showing the potential itself over the array for $(N,M)=(4,8)$ and $z=0.4$ (a) and 1.6 (b). The solid color in the center of B shows that as z increased beyond unity, the potential near the center is more uniform.

of former being the cathode plane of the latter. Issues remain about the optimal choice of the field of that boundary, and how to account for its small but nevertheless present variation with x and y , but those questions shall be taken up in a separate study. For present purposes, the 1D f is related to the 3D F_o via $f \propto F_o$ and $j \propto I_{tip}/a_{tt}^2$.

A demonstration of how rapidly the potential (or electric field) directly above a point charge converges with the potential (or electric field) above the midpoint of four point charges provides the final indication of how rapidly the ripples in Figs. 9 and 10 decline. As seen in Eq. (31) for the potential and Eq. (32) for the field, it will amount to finding numerically how rapidly the potentials off axis and on axis approach the same value. From Eq. (31), it is seen that such a question can be most easily answered by ignoring V_0 and evaluating

$$\begin{aligned} R_\varphi(z) &= \frac{\sum_{j^2+k^2 < M^2} \varphi_{jk}(0,0,z) + \delta_M}{\sum_{j^2+k^2 < M^2} \varphi_{jk}\left(\frac{1}{2}, \frac{1}{2}, z\right) + \delta_M} - 1, \\ R_F(z) &= \frac{\sum_{j^2+k^2 < M^2} \varphi'_{jk}(0,0,z) + \delta'_M}{\sum_{j^2+k^2 < M^2} \varphi'_{jk}\left(\frac{1}{2}, \frac{1}{2}, z\right) + \delta'_M} - 1. \end{aligned} \quad (35)$$

Equation (35) will approach 0 as z increases. It is seen that adding $4\pi\epsilon_0 a_{tt} V_0/\lambda$ to both the numerator and denominator in the fractional part (where the $M \rightarrow \infty$ limits give terms leading to the potential and field from R_φ and R_F , respectively) will only cause R_φ and R_F to decrease more rapidly. Therefore, Eq. (35) is a good metric to consider how the ripples fade. The terms δ_M and δ'_M , evaluated analogously to Eq. (34), appear in both the numerator and denominator, as for large M , whether $x=y=0$ or $1/2$ is of small importance. We find

$$\begin{aligned} \delta_M &= \frac{1}{2} \{ [M^2 + (N-z)^2]^{1/2} - [M^2 + z^2]^{1/2} \}, \\ \delta'_M &= \frac{1}{2} \left\{ \frac{z}{[M^2 + (N-z)^2]^{3/2}} + \frac{N-z}{[M^2 + z^2]^{3/2}} \right\}. \end{aligned} \quad (36)$$

The behavior of $R_\varphi(z)$ and $R_F(z)$ are shown in Fig. 11 as a function of z where M is taken to be 20 (for comparison, $M=10$ is also shown, and $N=10$ for both): it therefore is a

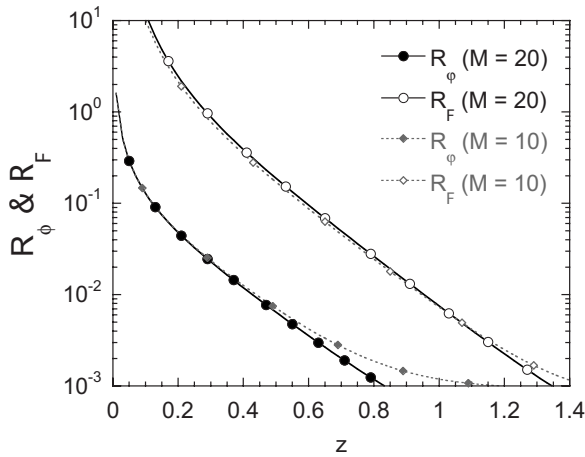


FIG. 11. Magnitude of the ripple amplitude functions R_ϕ and R_F as a function of distance z from the cathode surface, where z is in units of the tip-to-tip spacing of the array, for the “monopole” model of Eq. (35).

measure of the amplitude of the ripples of Fig. 9 and demonstrates the rapidity with which those ripples vanish. The field ripples vanish less rapidly than the potential ripples because ϕ' is more sensitive to variations than ϕ .

With a minor modification, it is possible to consider a cathode composed of sharper tips in a background field F_o . Let the cathode plane be at $z=0$ as before, but now consider two oppositely charged particles symmetrically placed about the z plane for each emitter which we shall call the “dipole” model (it anticipates the dipole model that shall be examined at length in the single-tip space charge investigation considered separately), in contrast to Eq. (35) that uses only one charge to represent the tip (“monopole” model). Therefore, the potential of the dipole in a background field is given by

$$V_{\text{dip}}(x, y, z) = F_o z + \frac{\lambda}{4\pi\epsilon_0 a_{\text{tip}}} \sum_{j=-\infty}^{\infty} \sum_{k=-\infty}^{\infty} \phi_{jk}^{\text{dip}}(x, y, z),$$

$$\phi_{jk}^{\text{dip}}(x, y, z) = \frac{1}{R_+} - \frac{1}{R_-},$$

$$R_{\pm} = [(j-x)^2 + (k-y)^2 + (z \pm d)^2]^{1/2}. \quad (37)$$

In other words, the anode at $z=N/2$ in the monopole model has been replaced by a background field F_o . As done with V_o in the monopole model, the background field F_o may be neglected in the dipole analog of Eq. (35), as the ratios minus 1 will be smaller with F_o than without it, and so the calculation without F_o serves as an upper bound. It is seen that the dipole model formulas for R_ϕ and R_F are obtained by the replacements $N \rightarrow 2d$ and $z \rightarrow z+d$ in the monopole formulas for R and δ , but the interpretations are different: d in the dipole model is smaller than the tip-to-tip spacing, whereas N in the monopole model is much greater than the tip-to-tip spacing. Performing the analogous calculation for the dipole model, the results are shown in Fig. 12 using $M=20$.

Gated structures

A final complication is the possible presence of a gate near the field emitter, which for field emitter array (FEAs)

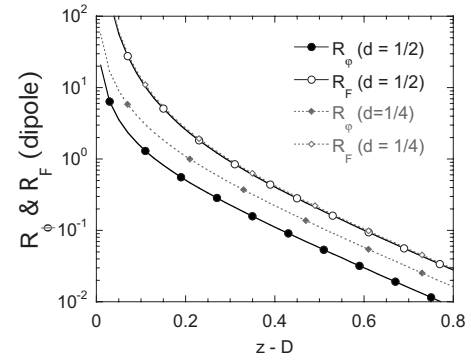


FIG. 12. Magnitude of the ripple amplitude functions R_ϕ and R_F as a function of distance $z-d$, where z is in units of the tip-to-tip spacing of the array, for the dipole model of Eq. (37).

serves to modulate the array: “emission-gated” current is required by a variety of technological applications from displays to microwave amplifiers⁹ and FELs.³¹ The simplest model of the gate (a metal plane collinear with the emitter apices from which disks centered about the emitter apex are excised, as shown in the expanded diagram in Fig. 8 of the gated cell) is to add to the charges that represent the emitter a charged ring to represent the gate (the so-called Saturn model⁴³). The potential is then, in spherical coordinates,

$$\varphi_{\text{saturn}}(r, \theta) = \frac{q}{4\pi\epsilon_0} \left\{ \frac{q_{\text{tip}}}{r} - \frac{q_{\text{ring}}}{r} \sum_{l=0}^{\infty} (-1)^l \frac{(2l)!}{2^{2l}(l!)^2} P_{2l}(\cos \theta) \right\}, \quad (38)$$

where $P_l(\cos \theta)$ is a Legendre polynomial, and where the magnitudes of the charges q_{tip} and q_{ring} are comparable. Therefore ϕ decreases faster than in the ungated case when the ring is absent, to leading order as $(q_{\text{tip}} - q_{\text{ring}})/r$, or, if $q_{\text{tip}} = q_{\text{ring}}$, as $2q_{\text{tip}}a_g^2/r^3$ for small θ . Therefore, an array of Saturn rings plus charges should coalesce more rapidly to the 1D representation than the ordered array of bare point charges considered previously.

For both gated and ungated geometries, an approach that may allow for the estimation of the impact of space charge on field emission from arrays in a manner amenable to PIC beam simulation codes is suggested. PIC is used to model the injection and acceleration of charge bunches especially when space charge complicates transport and causes emittance growth.^{19,44–48} Indeed, the needs of PIC codes suggest using the PCM approach to develop the cathode boundary of the PIC simulation. In so framing the problem, the space charge limits considered in the 1D section of this work have direct bearing to more comprehensive and time dependent PIC simulations, thereby allowing field emission sources to be treated by methods that in the past have been profitably used primarily on planar cathode structures.

UNIVERSAL FEATURES OF FIELD EMISSION IN 1D

In spite of its simplicity, the 1D CL model for a cathode of unlimited emissivity plays a very important role in the design and analysis of various devices¹ as well as for devel-

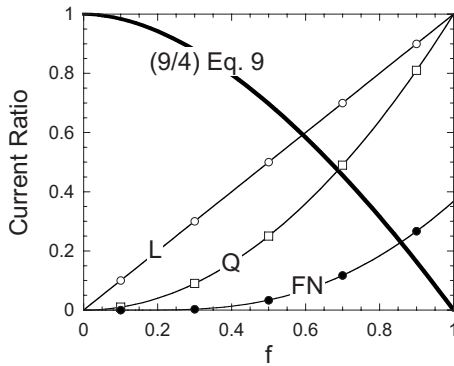


FIG. 13. The ratio of $9j/4$, where j is the ratio of current density with the CL limit, as a function of f (ratio of surface field F to vacuum field V_o/L) for various current-field relationships: L =linear; Q =quadratic, and FN =Fowler-Nordheim, for the cases $a=b=1$.

opening effective computational schemes for more realistic geometries. The situation is more complicated in the case of field emission because the current density depends on the field at the cathode surface, but surprisingly, Eq. (9) allows one to find universal features of emission which are independent of specific cathode properties [as also done by Forbes,¹⁷ who found a simplified version in his Eq. (15), although Eq. (9) here does not introduce extraneous roots]. As noticed by Forbes, and shown by Eq. (9), j is a function of f only, and, in particular, how close the current produced by field emission approaches the CL limit is determined solely by the field at the cathode surface (in units of the vacuum field). To show this, a plot of $9j/4$, with j given by Eq. (9), is compared to the example lines $j_l=f$, $j_q=f^2$, and $j_{FN}=f^2 \exp(-1/f)$ is shown in Fig. 13. The intersection points of the former with the three latter lines give the value of f that solves Eq. (9) for the particular current-field relation (linear, quadratic, or FN, respectively).

As demonstrated in Fig. 12, $9j/4 > 0.9$ as soon as $f < 0.27$ (alternately, $F < 0.27V_o/L$), and even when $f=1/2$, the current is not far from the CL limit ($9j/4 \approx 0.697$). The conclusion that a field with a magnitude of a quarter of the vacuum field V_o/L is sufficient to make emission almost equal to the CL limit can be observed in experiments. When $9j/4$ approaches unity and f approaches zero, then the following relationship is obtained from Eq. (9) for $F \ll V_o/L$,

$$F^2 \approx \left(\frac{8mq^2}{9\epsilon_0^2} \right)^{1/2} V_o^{1/2} [J_{CL}(V_o, L) - J(F)], \quad (39)$$

where we have returned to dimensioned units and use has been made of Eq. (5). Thus, for a given CL limit, F scales as $V_o^{1/4}$.

CONCLUSION

The relation of space charge to field emission is an important problem because of the strong variation in the emitted current with the field that exists at the emission site. Consequently, charge between anode and the emitter (or emitter-gate) boundary bears a complex relation to the voltages and separation distances defining the diode region. Three studies of space charge and its impact on field emission are therefore indicated. First, a 1D analysis of the basic

Poisson relation in a diode region is required. Second, a representation of a 3D field emitter structure adaptable to the 1D theory is needed. Third, and finally, a method to approximate the boundary needed in the 1D problem by considering the behavior of a 3D periodic array is needed. In the present study, the first and third issues have been addressed, and the second shall be reported separately. Although the present analysis is steady state, its results are commensurate with the asymptotic behavior of the PIC simulations of Feng and Verboncoeur.¹⁸ The transition from 3D to 1D for the case in which field emission arises from a surface that has irregularities or is purposely modified in such a way that the average spacing between the irregularities (spikes) is H , than at a height H above the surface of the cathode toward the anode, the electric field is indistinguishable from the 1D field, which is of consequence when cell-size constraints that are already important in PIC codes (e.g., Ref. 19) are an issue.

ACKNOWLEDGMENTS

The work of A.R. and J.L.L. was supported in part by AFOSR Grant No. AF-FA 9550-07; they thank Dr. R. Barker for useful discussions. The work of K.L.J. was supported provided by the *Naval Research Laboratory* and the *Joint Technology Office*; he thanks K. Nguyen (*Beam Wave Research*) and J. Petillo (*SAIC*) for useful discussions.

- ¹C. K. Birdsall and W. B. Bridges, *Electron Dynamics of Diode Regions* (Academic, New York, 1966).
- ²S. Humphries, *Charged Particle Beams* (Wiley, New York, 1990).
- ³M. Reiser, *Theory and Design of Charged Particle Beams* (Wiley, New York, 1994).
- ⁴J. S. Fraser and R. L. Sheffield, *IEEE J. Quantum Electron.* **23**, 1489 (1987).
- ⁵D. H. Dowell, K. J. Davis, K. D. Friddell, E. L. Tyson, C. a. Lancaster, L. Milliman, R. E. Rodenburg, T. Aas, M. Bemes, S. Z. Bethel, P. E. Johnson, K. Murphy, C. Whelen, G. E. Busch, and D. K. Remelius, *Appl. Phys. Lett.* **63**, 2035 (1993).
- ⁶P. Michelato, *Nucl. Instrum. Methods Phys. Res. A* **393**, 455 (1997).
- ⁷W. P. Dyke and J. Trolan, *Phys. Rev.* **89**, 799 (1953).
- ⁸E. L. Murphy and R. H. Good, *Phys. Rev.* **102**, 1464 (1956).
- ⁹W. Zhu, *Vacuum Microelectronics* (Wiley, New York, 2001).
- ¹⁰C. A. Spindt, I. Brodie, L. Humphrey, and E. R. Westerberg, *J. Appl. Phys.* **47**, 5248 (1976).
- ¹¹J. P. Barbour, W. Dolan, J. Trolan, E. Martin, and W. Dyke, *Phys. Rev.* **92**, 45 (1953).
- ¹²W. A. Anderson, *J. Vac. Sci. Technol. B* **11**, 383 (1993).
- ¹³R. L. Hartman, W. A. Mackie, and P. R. Davis, *J. Vac. Sci. Technol. B* **14**, 1952 (1996).
- ¹⁴K. L. Jensen, M. Kodis, R. Murphy, and E. Zaidman, *J. Appl. Phys.* **82**, 845 (1997).
- ¹⁵Y. Y. Lau, *Phys. Rev. Lett.* **87**, 278301 (2001).
- ¹⁶J. W. Luginsland, Y. Y. Lau, R. J. Umstatted, and J. J. Watrous, *Phys. Plasmas* **9**, 2371 (2002).
- ¹⁷R. G. Forbes, *J. Appl. Phys.* **104**, 084303 (2008).
- ¹⁸Y. Feng and J. Verboncoeur, *Phys. Plasmas* **13**, 073105 (2006).
- ¹⁹E. M. Nelson and J. J. Petillo, *IEEE Trans. Plasma Sci.* **32**, 1223 (2004).
- ²⁰K. L. Jensen, Y. Y. Lau, D. W. Feldman, and P. G. O'Shea, *Phys. Rev. ST Accel. Beams* **11**, 081001 (2008).
- ²¹K. L. Jensen, P. G. O'Shea, D. W. Feldman, and J. L. Shaw, *J. Appl. Phys.* **107**, 014903 (2010).
- ²²W. D. Jensen, F. B. Gerhard, Jr., and D. M. Koffman, in *Van Nostrand's Scientific Encyclopedia*, edited by G. D. Considine and P. H. Kulik (Wiley, New York, 2005), p. 1771.
- ²³P. Kruit, M. Bezuijen, and J. E. Barth, *J. Appl. Phys.* **99**, 024315 (2006).
- ²⁴M. J. Fransen, M. H. F. Overwijk, and P. Kruit, *Appl. Surf. Sci.* **146**, 357 (1999).
- ²⁵D. Morris, B. Gilchrist, and A. Gallimore, *AIP Conf. Proc.* **552**, 467

- (2001).
- ²⁶C. M. Marrese, J. E. Polk, K. L. Jensen, A. D. Gallimore, C. A. Spindt, R. L. Fink, and W. D. Palmer, in *Micropropulsion for Small Spacecraft*, edited by M. M. Micci and A. D. Ketsdever (American Institute of Aeronautics and Astronautics, Reston, VA, 2000), p. 18.
- ²⁷V. L. Granatstein, R. K. Parker, and C. M. Armstrong, *Proc. IEEE* **87**, 702 (1999).
- ²⁸R. K. Parker, R. H. Abrams, Jr., B. G. Danly, and B. Levush, *IEEE Trans. Microwave Theory Tech.* **50**, 835 (2002).
- ²⁹J. W. Lewellen and C. A. Brau, *Nucl. Instrum. Methods Phys. Res. A* **507**, 323 (2003).
- ³⁰J. W. Lewellen, in *Particle Accelerator Conference*, Proceedings of the IEEE Particle Acceleration Conference, 2005, p. 563.
- ³¹C. H. Boulware, J. D. Jarvis, H. L. Andrews, and C. A. Brau, *Int. J. Mod. Phys. A* **22**, 3784 (2007).
- ³²A. Rokhlenko and J. L. Lebowitz, *Phys. Plasmas* **11**, 4559 (2004).
- ³³A. Rokhlenko and J. L. Lebowitz, *Phys. Rev. Lett.* **91**, 085002 (2003).
- ³⁴R. H. Fowler and L. Nordheim, *Proc. R. Soc. London, Ser. A* **119**, 173 (1928).
- ³⁵K. L. Jensen, *J. Vac. Sci. Technol. B* **21**, 1528 (2003).
- ³⁶K. L. Jensen, *J. Appl. Phys.* **107**, 014905 (2010).
- ³⁷R. G. Forbes, *Appl. Phys. Lett.* **89**, 113122 (2006).
- ³⁸K. L. Jensen, *Advances in Imaging and Electron Physics*, Electron Emission Physics, Vol. 149 (Academic, New York, 2007).
- ³⁹K. L. Jensen, in *Vacuum Microelectronics*, edited by W. Zhu (Wiley, New York, 2001), p. 33.
- ⁴⁰R. G. Forbes, *J. Appl. Phys.* **103**, 114911 (2008).
- ⁴¹K. L. Jensen, *J. Appl. Phys.* **102**, 024911 (2007).
- ⁴²K. L. Jensen, P. Mukhopadhyay-Phillips, E. Zaidman, K. Nguyen, M. Kodis, L. Malsawma, and C. Hor, *Appl. Surf. Sci.* **111**, 204 (1997).
- ⁴³K. L. Jensen, E. Zaidman, M. Kodis, B. Goplen, and D. Smithe, *J. Vac. Sci. Technol. B* **14**, 1942 (1996).
- ⁴⁴L. Giannessi, *Phys. Rev. ST Accel. Beams* **6**, 114802 (2003).
- ⁴⁵R. A. Kishek, S. Bernal, C. L. Bohn, D. Grote, I. Haber, H. Li, P. G. O'Shea, M. Reiser, and M. Walter, *Phys. Plasmas* **10**, 2016 (2003).
- ⁴⁶J. J. Petillo, E. M. Nelson, J. F. Deford, N. J. Dionne, and B. Levush, *IEEE Trans. Electron Devices* **52**, 742 (2005).
- ⁴⁷K.-J. Kim, B. Carlsten, D. Dowell, K. Flottmann, K. Jensen, J. Petillo, A. Sessler, and G. Stupakov, ANL/APS/LS-305 <http://www.osti.gov/energycitations/servlets/purl/834030-AxIERG/native/> (2004).
- ⁴⁸D. A. Dimitrov, D. I. Bruhwiler, J. R. Cary, P. Messmer, P. Stoltz, K. L. Jensen, D. W. Feldman, and P. G. O'Shea, in *Particle Accelerator Conference*, Proceedings of the IEEE Particle Acceleration Conference, 2005, p. 2583.